J|A|C|S
ARTICLES
Published on Web 12/16/2005

Magnetic Coupling in Dinuclear Gd Complexes

Lindsay E. Roy and Timothy Hughbanks*

Contribution from the Department of Chemistry, Texas A&M University, P.O. Box 30012, College Station, Texas 77842-3012

Received August 17, 2005; E-mail: trh@mail.chem.tamu.edu

Abstract: A spin density functional (SDFT) study of carboxylate-bridged and diazenido-bridged dinuclear gadolinium compounds is presented. Calculated magnetic coupling constants for the carboxylate-bridged structures are in good agreement with experimental data, confirming the ability of the broken symmetry approach used in this work to predict magnetic behavior in such compounds. The systematic trend wherein symmetrically bridged complexes are antiferromagnetically coupled and asymmetrically bridged are ferromagnetically coupled is reproduced by the SDFT calculations. The mechanism underlying magnetic coupling in closed- and open-shell dinuclear complexes is described using a perturbative molecular orbital model that focuses the influence of the $4f^7$-5*d* exchange interaction on molecular orbitals with significant 5*d*-orbital character for the complex $[\{[(Me_3Si)_2N]_2(thf)Gd\}_2(N_2)]$. Open-shell electronic configurations facilitate strong ferromagnetic coupling, whereas in closed-shell systems antiferromagnetic coupling is usually preferred.

Introduction

Theoretically derived rules for interpreting and designing magnetic molecules and materials that incorporate organic radicals and/or transition metal ions have been conceived and refined over many years and serve an important guide for experimentalists who synthesize and measure the properties of magnetic materials.[1−14] The synthesis of an expanded class of Prussian blues and interpretation of their magnetic properties by the groups of Girolami, Long, and Verdaguer, for example, were clearly guided by an understanding of the orbital interactions responsible for ferro- and antiferromagnetic coupling in these network solids.[15−28]

In recent years, an increasing number of chemists have turned their attention to molecules and hybrid organic−inorganic materials (e.g., coordination network solids) that incorporate magnetic lanthanide ions.[29−32] For the most part, these efforts have proceeded in an empirical fashion because coordination chemists have not been guided by theoretical criteria for "building in" magnetic coupling between paramagnetic lanthanide ions. Indeed, it is unclear whether it is possible to make coordination networks to manifest appreciable coupling.

In this contribution, we subject dinuclear gadolinium complexes with bridging carboxylate, phenoxide, and diazenido bridging ligands to theoretical scrutiny with the purpose of learning how intervening ligands in these complexes influence the magnetic coupling between the gadolinium $4f^7$ (^{8}S) ion cores. As the preceding comments indicate, our purpose is to elucidate electronic factors that might be transferable to polynuclear lanthanide-containing molecules and materials that might exhibit magnetic ordering.

There are, of course, materials where relatively strong magnetic coupling of lanthanide moments *does* occur: in the

(1) Goodenough, J. B. *Magnetism and the Chemical Bond*; Interscience Publishers: New York, 1963; Vol. I.
(2) Hay, P. J.; Thibeault, J. C.; Hoffmann, R. *J. Am. Chem. Soc.* **1975**, *97*, 4884.
(3) Kahn, O.; Briat, B. *J. Chem. Soc., Faraday Trans.* **1976**, *72*, 1441.
(4) Kahn, O. *Molecular Magnetism*; VCH: New York, 1993.
(5) Christou, G.; Gatteschi, D.; Hendrickson, D. N.; Sessoli, R. *Mater. Res. Soc. Bull.* **2000**, *25*, 66.
(6) Gatteschi, D. *J. Alloys Compd.* **2001**, *317−318*, 8.
(7) Ruiz, E.; Alemany, P.; Alvarez, S.; Cano, J. *J. Am. Chem. Soc.* **1997**, *119*, 1297.
(8) Ruiz, E.; Alvarez, S. *J. Chem. Soc., Chem. Commun.* **1998**, 2767.
(9) Ruiz, E.; Alvarez, S.; Rodriguez-Fortea, A.; Alemany, P.; Pouillon, Y.; Massobrio, C. In *Magnetism: Molecules to Materials II*; Miller, J. S., Drillon, M., Eds.; Wiley-VCH: Weinheim, New York, 2001; p 227.
(10) Gillon, B.; Mathoniere, C.; Ruiz, E.; Alvarez, S.; Cousson, A.; Rajendiran, T. M.; Kahn, O. *J. Am. Chem. Soc.* **2002**, *124*, 14433.
(11) Desplanches, C.; Ruiz, E.; Alvarez, S. *Eur. J. Inorg. Chem.* **2003**, 1756.
(12) Paulovic, J.; Cimpoesu, F.; Ferbinteanu, M.; Hirao, K. *J. Am. Chem. Soc.* **2004**, *126*, 3321.
(13) Whangbo, M. H.; Koo, H. J. *Inorg. Chem.* **2002**, *41*, 3570.
(14) Dai, D.; Whangbo, M.-H. *J. Chem. Phys.* **2003**, *118*, 29.
(15) Mallah, T.; Ferlay, S.; Sculler, A.; Verdaguer, M. *NATO Adv. Study Inst. Ser., Ser. C* **1996**, *484*, 597.
(16) Verdaguer, M.; Bleuzen, A.; Marvaud, V.; Vaissermann, J.; Seuleiman, M.; Desplanches, C.; Sculler, A.; Train, C.; Garde, R.; Gelly, G.; Lomenech, C.; Rosenman, I.; Veillet, P.; Cartier, C.; Villain, F. *Coord. Chem. Rev.* **1999**, *190−192*, 1023.
(17) Bennett, M. V.; Beauvais, L. G.; Shores, M. P.; Long, J. R. *J. Am. Chem. Soc.* **2001**, *123*, 8022.
(18) Shores, M. P. Ph.D. Dissertation, 2002.
(19) Beauvais, L. G.; Long, J. R. *J. Am. Chem. Soc.* **2002**, *124*, 12096.
(20) Tulsky, E. G.; Crawford, N. R. M.; Baudron, S. A.; Batail, P.; Long, J. R. *J. Am. Chem. Soc.* **2003**, *125*, 15543.
(21) Yan, B.; Zhou, H.; Lachgar, A. *Inorg. Chem.* **2003**, *42*, 8818.
(22) Goodenough, J. B. *Struct. Bonding (Berlin)* **2001**, *98*, 1.
(23) Daul, C. A.; Ciofini, I.; Bencini, A. In *Reviews of Modern Quantum Chemistry*; Sen, K. D., Ed.; World Scientific: Singapore, River Edge, N.J., 2002; Vol. 2, p 1247.
(24) Veciana, J.; Iwamura, H. *MRS Bull.* **2000**, *25*, 41.
(25) Rovira, C., *Struct. Bonding (Berlin)* **2001**, *100*, 163.
(26) Iwamura, H.; Inoue, K. *Magnetism: Molecules to Materials II*; Miller, J. S., Drillon, M., Eds.; Wiley-VCH: Weinheim, New York, 2001; p 61.
(27) Rajca, A. *Mol. Cryst. Liq. Cryst. Sci. Technol., Sect. A* **1997**, *305*, 567.
(28) Rajca, S.; Rajca, A. *J. Solid State Chem.* **2001**, *159*, 460.
(29) Cui, H.; Otsuka, T.; Kobayashi, A.; Takeda, N.; Ishikawa, M.; Misaki, Y.; Kobayashi, H. *Inorg. Chem.* **2003**, *42*, 6114.
(30) Ishikawa, N.; Sugita, M.; Ishikawa, T.; Koshihara, S.-Y.; Kaizu, Y. *J. Am. Chem. Soc.* **2003**, *125*, 8694.
(31) Buenzli, J.-C. G.; Piguet, C. *Chem. Rev.* **2002**, *102*, 1897.
(32) Benelli, C.; Gatteschi, D. *Chem. Rev.* **2002**, *102*, 2369.

10.1021/ja055035j CCC: $33.50

elemental metals and in intermetallic compounds, especially those with the "magnetic" transition metals (Fe, Co, and Ni).[33−39] Indeed, the general characteristics of these systems provide some initial hints as to what molecular systems might offer particular promise.

To a much greater extent than the *d* orbitals on transition metal atoms, the 4*f* orbitals on lanthanide atoms are highly contracted, and their direct participation in magnetic superexchange coupling (mediated by 4*f*-overlap with intervening ligand orbitals) is effectively precluded.[4,40] In rare-earth intermetallic compounds, however, an indirect pathway involving the localized 4*f* electrons and the conduction electrons is responsible for magnetic ordering.[41−44] Elemental gadolinium, for example, is a metallic ferromagnet that orders near ambient temperature. The $4f^7$ moments are coupled through an indirect mechanism, in which the 5*d* conduction electrons mediate 4*f*−4*f* coupling.[45−47] When the conduction electrons are spin-polarized, as in Fe-rich or Co-rich intermetallic compounds that contain lanthanides (e.g., $Nd_2Fe_{14}B$ and $SmCo_5$), the exchange coupling to the conduction electrons can be even stronger—with the lanthanide moment alignment remaining "fixed" by the surrounding polarized spin density.[41,48,49]

Computational Methods for Lanthanide Complexes

Broken Symmetry Approach. The exchange interaction between two paramagnetic centers is phenomenologically described using the Heisenberg−Dirac−Van Vleck (HDVV) spin Hamiltonian;[50−52]

$$\hat{H} = -J_{ij}\hat{S}_i\hat{S}_j \tag{1}$$

where J_{ij} is the magnetic coupling constant describing the spin exchange between different spin states and $\hat{S}_i$ and $\hat{S}_j$ are the total spin operators for atoms *i* and *j*. The effective Hamiltonian is defined such that the sign of the magnetic coupling constant, J_{ij}, is positive for ferromagnetic coupling and negative for an antiferromagnetic interaction.

The spin eigenfunction of the high-spin state for $|SM_S\rangle$ is a single Slater determinant (where *S* is the total spin and M_S is its *z*-component). Any lower-spin state eigenfunction is expressed as linear combinations of Slater determinants and therefore is not amenable to direct calculation in the usual implementation of density functional theory. Noodleman *et al.* have proposed an alternative approach, in which unrestricted, or spin-polarized, functions are evaluated within the density functional formalism and the expectation value(s) for broken symmetry solution(s) is(are) used in calculating the energy of the low-spin state(s).[53−55] The coupling constant of dinuclear complex is evaluated using the energy difference between the high-spin state and the computed expectation value (energy) of the low-spin, broken symmetry determinant. For the case in which $S_i = S_j$, the coupling constant may be obtained by use of eq 2;[56]

$$E_{HS} - E_{LS} = -2JS_i(S_i + 1/2) \tag{2}$$

where E_{HS} is the energy that corresponds to the state with the highest total spin, E_{LS} corresponds to the state with the lowest total spin ($S = 0$, for a homodinuclear complex), and S_i is the total spin on each metal atom. Experience has shown that estimating the energy of the low-spin state by making use of the computed "energy" for the broken symmetry solution for transition metal complexes without performing any spin projection, leads to good agreement with experimental data for a large variety of compounds with exchange coupled electrons.[7,8,11,14,57−63]

In applying the symmetry-broken approach to a molecule with two Gd centers, spin density functional theory (SDFT) is first used to calculate the energy of $|\uparrow_7,\uparrow_7\rangle$ and $|\uparrow_7,\downarrow_7\rangle$.[64] The former spin eigenfunction represents a state with all seven of the *f*-electrons on both Gd atoms spin up and the latter expression, $|\uparrow_7,\downarrow_7\rangle$, represents a determinant where all seven *f*-electrons on one Gd atom are spin up and all seven on the other Gd atom are spin down, which is a combination of pure spin determinants with $S = 0, 1, ..., 7$ and $M_S = 0$. The energy of the high spin state can be identified with the energy obtained with the HDVV Hamiltonian ($\hat{H} = -J\hat{S}_1\cdot\hat{S}_2$):$E|\uparrow_7,\uparrow_7\rangle = -49/4\ J$. Overlaps between *f* orbitals on neighboring atoms are very small, e.g., $\langle\downarrow_7,\uparrow_7|\uparrow_7,\downarrow_7\rangle \approx 0$, so $|\uparrow_7,\downarrow_7\rangle$ can be expressed as a combination of pure states using the Clebsch−Gordan coefficients without overlap corrections, and its energy can be obtained using the same coefficients:

$$E_{|\uparrow_7,\downarrow_7\rangle} = \frac{3}{24}E_0 + \frac{7}{24}E_1 + \frac{7}{24}E_2 + \frac{49}{264}E_3 + \frac{7}{88}E_4 + \frac{7}{312}E_5 + \frac{1}{264}E_6 + \frac{1}{3432}E_7 \tag{3}$$

The HDVV Hamiltonian yields an energy expression in terms of the set of pure state energies ($E_S = (J/4)(S(S+1))$):

$$E_{|\uparrow_7,\downarrow_7\rangle} = \frac{49}{4}J \Rightarrow \frac{49}{2}J = E_{|\uparrow_7,\downarrow_7\rangle} - E_{|\uparrow_7,\uparrow_7\rangle} \tag{4}$$

An identical value for $E_{|\downarrow_7,\uparrow_7\rangle}$ is obtained from the expectation value, $\langle|\uparrow_7,\downarrow_7\rangle|\hat{H}||\uparrow_7,\downarrow_7\rangle$, *directly* and this is how one can correlate computed SDFT energies with coupling parameters *in practice*; the point of these comments being a demonstration of the equivalence of this procedure with the broken-symmetry approach.

(33) Kremer, R. K.; Simon, A. *J. Less-Common Met.* **1987**, *127*, 262.
(34) Simon, A.; Mattausch, H. J.; Miller, G. J.; Bauhofer, W.; Kremer, R. K. In *Handbook on the Physics and Chemistry of Rare Earths*; Gschneidner, K. A.; Eyring, L., Eds.; Elsevier Science: New York, 1991; Vol. 15, p 191.
(35) Simon, A., *J. Alloys Compd.* **1995**, *229*, 158.
(36) Kasten, A.; Muller, P. H.; Schienle, M. *Solid State Commun.* **1984**, *51*, 919.
(37) Felser, C.; Ahn, K.; Kremer, R. K.; Seshadri, R.; Simon, A. *J. Solid State Chem.* **1999**, *147*, 19.
(38) Hughbanks, T.; Corbett, J. D. *Inorg. Chem.* **1988**, *27*, 2022.
(39) Meng, F.; Sweet, L.; Hughbanks, T. Unpublished results.
(40) Carlin, R. L. *Magnetochemistry*; Springer-Verlag: Berlin, 1989.
(41) Wallace, W. E. *Prog. Solid State Chem.* **1985**, *16*, 127.
(42) Elliot, R. J. In *Magnetic Properties of Rare Earth Metals*; Elliot, R. J., Ed.; Plenum Publishing: New York, 1972; p 425.
(43) Koehler, W. C. In *Magnetic Properties of Rare Earth Metals*; Elliot, R. J., Ed.; Plenum Publishing: New York, 1972; p 81.
(44) Rhyne, J. J. In *Magnetic Properties of Rare Earth Metals*; Elliot, R. J., Ed.; Plenum Publishing: New York, 1972; p 129.
(45) Ruderman, M. A.; Kittel, C. *Phys. Rev. B: Condens. Matter* **1954**, *96*, 99.
(46) Kasuya, T. *Prog. Theor. Phys. (Japan)* **1956**, *16*, 45.
(47) Yosida, K. *Phys. Rev. B: Condens. Matter* **1957**, *106*, 893.
(48) Fidler, J. *Inst. Phys. Conf. Ser.* **1998**, *152*, 805.
(49) Radwanski, R. J.; Michalski, R.; Ropka, Z.; Blaut, A. *Phys. B: Condens. Matter* **2002**, *319*, 78.
(50) Heisenberg, W., *Z. Phys.* **1928**, *49*, 619.
(51) Dirac, P. A. M. *Proc. R. Soc. (London)* **1929**, *A123*, 714.
(52) Van Vleck, J. H. *The Theory of Electric and Magnetic Susceptibilities*; The Clarendon: Oxford, 1932.
(53) Noodleman, L. *J. Chem. Phys.* **1981**, *74*, 5737.
(54) Noodleman, L.; Case, D. A. *Adv. Inorg.Chem.* **1992**, *38*, 423.
(55) Li, J.; Noodleman, L.; Case, D. A. In *Inorganic Electronic Structure and Spectroscopy*; Solomon, E. I., Lever, A. B. P., Eds.; Wiley: New York, 1999; Vol. 1, p 661.
(56) Rodriguez-Fortea, A.; Alemany, P.; Alvarez, S.; Ruiz, E.; Scuiller, A.; Decroix, C.; Marvaud, V.; Vaissermann, J.; Verdaguer, M.; Rosenman, I.; Julve, M. *Inorg. Chem.* **2001**, *40*, 5868 and references therein.
(57) Ruiz, E.; Alemany, P.; Alvarez, S.; Cano, J. *Inorg. Chem.* **1997**, *36*, 3683.
(58) Cano, J.; Alemany, P.; Alvarez, S.; Verdaguer, M.; Ruiz, E. *Chem. Eur. J.* **1998**, *4*, 476.
(59) Ruiz, E.; Cano, J.; Alvarez, S.; Alemany, P. *J. Comput. Chem.* **1999**, *20*, 1391.
(60) Davidson, E. R.; Clark, A. E. *J. Phys. Chem. A* **2002**, *106*, 7456.
(61) Angaridis, P. A.; Baran, P.; Boca, R.; Cervantes-Lee, F.; Haase, W.; Mezei, G.; Raptis, R. G.; Werner, R. *Inorg. Chem.* **2002**, *41*, 2219.
(62) Rodriguez-Fortea, A.; Ruiz, E.; Alemany, P.; Alvarez, S. *Monatsh. Chem.* **2003**, *134*, 307.
(63) Ruiz, E.; Cano, J.; Alvarez, S.; Caneschi, A.; Gatteschi, D. *J. Am. Chem. Soc.* **2003**, *125*, 6791.
(64) Roy, L.; Hughbanks, T. *J. Solid State Chem.* **2003**, *176*, 294.

To qualitatively assess whether any particular system will exhibit ferro- or antiferromagnetic coupling, it is useful to examine the characteristics of the broken-symmetry solution, $|\uparrow_7,\downarrow_7\rangle$, even though it does not actually represent any (single) spin eigenfunction. Whatever factors one can identify that tend to (de)stabilize $|\uparrow_7,\downarrow_7\rangle$ versus $|\uparrow_7,\uparrow_7\rangle$ (a true spin eigenfunction) will proportionately affect the (de)stabilization of the true low-spin eigenfunction. In the discussion below, we shall discuss certain characteristics of broken symmetry determinant(s), such as spin polarization of Gd 6*s* and 5*d* electrons induced by the $4f^7$ core electrons, to gain insight into the origin of magnetic coupling in dinuclear complexes. It should be borne in mind that the correct symmetrized low-spin wave functions do not exhibit any net spin polarization because they contain, among other terms, equal contributions from $|\uparrow_7,\downarrow_7\rangle$ and $|\downarrow_7,\uparrow_7\rangle$—and the spin polarization in each is offset by the other.

Computational Details. The GGA/BLYP density functional has been used in all Gd calculations as implemented in DMol^3 within the Cerius2 suite of programs.[65−67] This uses Becke's expression for the exchange functional,[68] and the Lee−Yang−Parr correlation functional.[69] The double numerical (DND) basis including *d*-polarization functions was employed in DMol^3 calculations for all atoms. A small frozen-core (1*s*2*s*2*p*3*s*3*p*3*d*) effective potential was used for Gd. All calculations included scalar relativistic effects and open-shell configurations. The convergence criterion for the energy was set at 10^{-6} au. In all calculations, we have employed 302 radial points, generated with a harmonic function with $l = 29$ (called a "fine grid" in DMol^3). To check the influence of the grid on the accuracy of the results, we performed some test calculations increasing the size up to $l = 41$. The difference in the 2*J* values computed with the two grids was ~0.002 cm^{-1}, and thus the use of the fine grid was deemed to be acceptable.

Since modest changes with respect to the experimental structure can sometimes result in significant changes in the computed coupling constant, we used the experimental molecular structures, rather than optimized structures, when available. Geometries were optimized at the DFT/BLYP level with TZ2P small core basis sets using relativistic scalar zero-order-regular approximation (ZORA) method in the Amsterdam density functional (ADF) package.[70,71] The Dirac utility was used to generate relativistic frozen core potentials for the scalar ZORA calculations. The integration parameter *accint* and the energy convergence criterion were set at 6 and 10^{-6} au, respectively. Symmetry was lifted in all calculations.[72]

Geometries used in calculations of phenoxide- and carboxylate-bridged dinuclear compounds were based on structures of related compounds determined by X-ray crystallography. When necessary, experimental structures were slightly idealized to achieve inversion symmetry. Partial geometry optimizations were performed on the two models mimicking the heptadentate amino phenoxide Gd complex bis((μ_2-tris-(((2-Hydroxybenzyl)amino)ethyl)amine)gadolinium), ([Gd(AmPh)]$_2$), in which the models contain either one bridging phenoxide group, Ph = 3 and Ph = 1, or a bridging enolate group, Ph = 0 (refer to Figure 3 for notation). In both cases, the Gd−L distances and angles were kept at experimentally determined values, and only the ligands were optimized.

Since no diazenido-bridged dinuclear gadolinium complexes have been reported, its structure was obtained from a yttrium analogue by multiplying observed Y−L distances by a scale factor of 1.029—the ratio of the two metals' 8-coordinate crystal radii—to obtain Gd−L distances.[73] Geometries of the yttrium diazenido complexes were also optimized at the DFT/BLYP level. Partial geometry optimizations for the one-electron oxidized product were performed using both experimental and optimized geometries, keeping constant the distances and angles of the bis(silyl)amide and solvent ligands. Both yielded the same geometry. In discussions referring to van der Waals (v-d-W) radii, standard radii were taken for C (1.70 Å), Si (2.10 Å), and N (1.55 Å).[74] For yttrium, the v-d-W radius (2.42 Å) was obtained using the relation $R_{vdw} = R_{cov} + 0.80$ Å with $R_{cov} = 1.62$ Å. A standard Mulliken population analysis was carried out to obtain total atomic populations and charges.

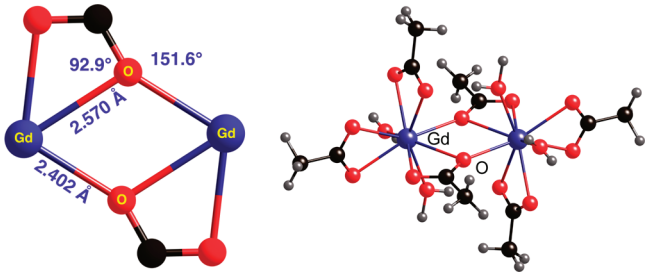

Figure 1. Structure of [Gd(OAc)$_3$(H$_2$O)$_2$]$_2$ and detail of the Gd$_2$O$_2$ core.

In magnetic-coupling calculations of lanthanide complexes and solids, the simplest nontrivial element to treat is gadolinium, where *f*−*f* spin−orbit coupling effects are absent in first order (for the ^{8}S state of the $4f^7$ core) and can therefore be safely neglected. As we have discussed in previous work, the calculated gap between the ground ^{9}D and lowest excited ^{7}D Gd-atomic states ($4f^7 5d^1 6s^2$ configuration), using the BLYP functional and the double numeric basis sets discussed above, is about 89% of the spectroscopically measured gap (0.793 eV), after accounting for spin contamination and averaging over spin−orbit splitting in both states.[64] A well-known artifact of DFT should be acknowledged:[75] although both states are orbitally degenerate, their energies, computed with all current functionals, depend slightly on which *d* orbital is actually occupied. In our calculations, we examined the $E(^7\text{D}) - E(^9\text{D})$ difference by occupying one of the four spatially equivalent "cloverleaf" orbitals (i.e., not d_{z^2}) in both states, and the energy difference given reflects this choice.

Benchmark Systems: Alkoxo-Bridged Gd(III) Dinuclear Complexes

[Gd(OAc)$_3$(H$_2$O)$_2$]$_2$. [{Gd(OAc)$_3$(H$_2$O)$_2$}$_2$]·4H$_2$O (**1**) has a structure wherein two of the six carboxylate units bridge each gadolinium to form a planar four-membered ring.[76] In the bridging acetate ligands, the oxygen atoms not involved in the central Gd$_2$O$_2$ parallelogram bind to one Gd center, as shown in Figure 1. Two additional acetate ions and water molecules complete the coordination environment around each Gd^{3+} ion. The distance between the gadolinium ions within the dinuclear unit is 4.206 Å, and the angles at the oxygen bridgeheads are 115.48°. [{Gd(OAc)$_3$(H$_2$O)$_2$}$_2$] exhibits ferromagnetic coupling; the effective moment (per Gd) reaches 9.07 μ_B at 1.74 K, and the susceptibility data is fit with $J = 0.03$ cm^{-1}.[77]

[Gd(AmPh)]$_2$. [Gd(AmPh)]$_2$·2CHCl$_3$ (**2**) is a homodinuclear complex containing two 8-coordinate Gd ions, each of which

(65) Delley, B. *J. Chem. Phys.* **1990**, *92*, 508.
(66) Delley, B. *J. Chem. Phys.* **2000**, *113*, 7756.
(67) Delley, B. *Comput. Mater. Sci.* **2000**, *17*, 122.
(68) Becke, A. D. *Phys. Rev. A: At. Mol. Opt. Phys.* **1988**, *38*, 3098.
(69) Lee, C.; Yang, W.; Parr, R. G. *Phys. Rev. B: Condens. Matter* **1988**, *37*, 785.
(70) Te Velde, G.; Bickelhaupt, F. M.; Baerends, E. J.; Fonseca Guerra, C.; Van Gisbergen, S. J. A.; Snijders, J. G.; Ziegler, T. *J. Comput. Chem.* **2001**, *22*, 931.
(71) *ADF2003.01. SCM, Theoretical Chemistry*; Vrije Universiteit: Amsterdam, The Netherlands (see Supporting Information for the complete reference).
(72) Users of the ADF program using Symmetry option should be certain that the parameter A1FIT is set high enough (for example, 10 Å) to avoid errors that this method can otherwise introduce.
(73) Ganguly, P. *J. Am. Chem. Soc.* **1993**, *115*, 9287.
(74) Bondi, A. *J. Phys. Chem.* **1964**, *68*, 441.
(75) Koch, W.; Holthausen, M. C. *A Chemist's Guide to Density Functional Theory*; 2nd ed.; Wiley-VCH: New York, 2000; p 294.
(76) Hatscher, S. T.; Urland, W. *Angew. Chem., Int. Ed.* **2003**, *42*, 2862.
(77) It is worth emphasizing, here and subsequently, that this corresponds to an energy difference between $|\uparrow_7,\uparrow_7\rangle$ and $|\uparrow_7,\downarrow_7\rangle$ of ~0.75 cm^{-1} (see eq 3).

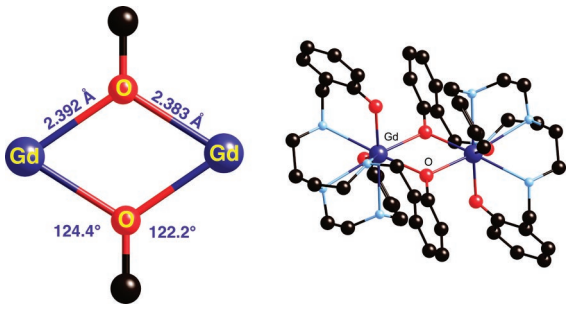

Figure 2. Structure of $[Gd(AmPh)]_2$ and detail of the Gd_2O_2 core.

Table 1. Exchange Coupling Constants $2J$ (cm^{-1}) Calculated as the ($S = 0$) − ($S = 7$) Energy Difference for the Structures of the Oxo-Bridged Gd(III) Dinuclear Complexes and Related Model Structures

complex	J_{Calcd}	J_{Exptl}
	$[Gd(O_2CH)_2(\mu{-}O_2CR)(H_2O)_2]_2$	
$R = CH_3$	0.053	0.039
$R = CF_3$	0.046	
$R = H$	0.040	
	$[Gd(AmPh)]_2$	
Ph = 3	−0.116	−0.045
Ph = 1	−0.116	
Ph = 0	−0.121	

is coordinated by (tris(((2-hydroxybenzyl)amino)ethyl)amine (AmPh), a triply deprotonated heptadentate Schiff base ligand (Figure 2).[78] One phenolate arm on each ligand acts as a bridge between the two metal centers, which are separated by 3.984 Å; the angle at the oxygen bridgeheads is 113.12°. The molecule is centrosymmetric, and the Gd_2O_2 parallelogram is nearly rhombic (the two Gd−O distances are 2.391(2) and 2.384(2) Å). The complex exhibits antiferromagnetic coupling with a decrease in the magnetic moment with temperature such that the moment (per Gd) falls to 7.30 μ_B at 4.2 K (derived coupling constant, $J = -0.045$ cm^{-1}).

The experimental and calculated exchange coupling constants for complexes **1** and **2** and related models are shown in Table 1. Although they lack quantitative accuracy, our calculations successfully predict the qualitative nature of the coupling (i.e., the sign of J) and give good agreement for the magnitude of the coupling in every case, which is always very small. To check the applicability of our computational models to correctly evaluate coupling constants in real compounds, we calculated J for different model structures using the experimentally determined structural data for both compounds. Results for other carboxylate derivatives based on **1** indicate that electron-withdrawing groups exert little influence on the strength of exchange; all of the cases computed are predicted to have coupling constants very similar to that found for acetate bridges.[79]

For the models of complex **2** (see Figure 3), simplifying only the terminal phenoxide groups of the heptadentate ligand and maintaining the phenolate bridge yields a computed constant of −0.116 cm^{-1} [that is larger than experimentally observed (−0.045 cm^{-1})] but correctly predicts antiferromagnetic coupling. Similarly, when replacing the bridging phenoxide group with a model using enolate bridges, one observes a larger calculated coupling constant (−0.121 cm^{-1}) than that for the experimental model; however, it correctly predicts weak antiferromagnetic coupling of comparable magnitude as the other calculated coupling constants.

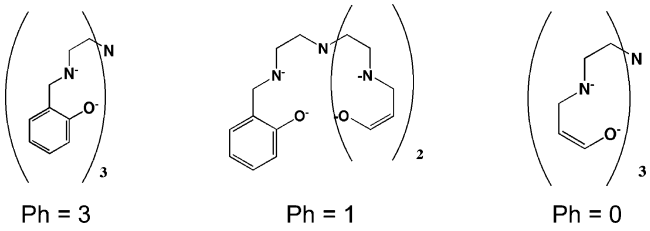

Figure 3. Model structures for $[Gd(AmPh)]_2$. Ph = 3 refers to a ligand with three phenoxide groups, Ph = 1 refers to a Gd_2-bridging ligand with one phenoxide group, and Ph = 0 refers to a bridging ligand with no phenoxide moieties.

The important distinction between these two classes of complexes is in the geometries of the Ln_2O_2 carboxylate (phenolate) bridges. The central Ln_2O_2 cores of the phenolate-bridged complexes, **2**, show near-D_{2h} symmetry: all the Ln−O bond distances are nearly equal, and the Ln−O−C(ring) angles are all within 2° of their mean values. In contrast, the Ln_2O_2 cores of the carboxylate-bridged molecules, **1**, have approximate C_{2h} symmetry: the Ln−O lengths show significant alternation within the Ln_2O_2 ring, and the lines containing the *exo*-O−C do not radiate outward from the center of the ring (see Figures 1 and 2). The differences computed in all of our calculations seem to correlate with the donor ability of the ligand and the break in symmetry. In addition to a large in-plane displacement, the oxygen bridgehead angles are also important for assessing the coupling exhibited by the Gd centers (**1**). Small increases in Gd−O−Gd angle, θ, appear to favor ferromagnetic exchange. Also, as the in-plane angle, φ, tends toward 120°, the system exhibits antiferromagnetic character. These small changes, however, are not as substantial as the ligand effect on lowering the symmetry.

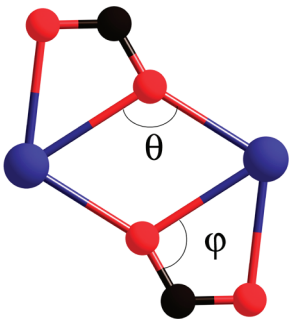

Magnetostructural Correlations in Alkoxo-Bridged Gd(III) Dinuclear Complexes

Gd−O distances for other alkoxo-bridged Gd(III) dinuclear complexes range between 2.940 and 2.324 Å. To investigate the correlation between the Gd−O distance and magnetic coupling, we calculated the coupling constant for several model structures with a Gd_2O_2 ring.[76,78,80−83] The calculated values of

(78) Liu, S.; Gelmini, L.; Rettig, S. J.; Thompson, R. C.; Orvig, C. *J. Am. Chem. Soc.* **1992**, *114*, 6081.
(79) Urland and authors published the single-crystal structures and magnetic behavior of $Gd(HF_2CCOO)_3(H_2O)_2{\cdot}2H_2O$ and $Gd(H_3CCOO)_3(H_2O)_2{\cdot}2H_2O$, showing antiferromagnetic coupling for the former and ferromagnetic coupling for the latter. This structure type is different from the one in this study. Rohde, A.; et al. *J. Alloys Compd.* **2004**, *374*, 137.
(80) Hernandez-Molina, M.; Ruiz-Perez, C.; Lopez, T.; Lloret, F.; Julve, M. *Inorg. Chem.* **2003**, *42*, 5456.
(81) Costes, J.-P.; Clemente Juan, J.-M.; Dahan, F.; Nicodeme, F. *J. Chem. Soc., Dalton Trans.* **2003**, 1272.

Table 2. Exchange Coupling Constants $2J$ (cm^{-1}) Calculated from the ($S = 0$) − ($S = 7$) Energy Difference for Various Oxo-Bridged Gd(III) Dinuclear Complexes

compound	θ/deg	φ/deg	Gd···Gd (Å)	Gd–O (Å)	J_{exp}	J_{calc}	ref
$[Gd_2(mal)_2(H_2O)_6]$	116.71	92.59	4.277	2.426/2.597	0.048	0.057	80
$[Gd_2(acetylsal)_4]_\infty$	114.3	94.0	4.187	2.439/2.545	0.037	0.075	81
$[\{Gd(OAc)_3(H_2O)_2\}_2]$	115.48	92.88	4.206	2.403/2.570	0.03	0.039	76
$[Gd_2(O_2Fc)_2(O_2Fc)_4(MeOH)_2]$	112.44	83.39	4.409	2.349/2.941	0.006	0.003[a]	82
$[Gd(AmPh)]_2$	113.12	124.41	3.984	2.383/2.392	−0.045	−0.116	78
$[\{Gd(Hsabhea)(NO_3)\}_2]$	107.61	121.01	3.764	2.324/2.341	−0.198	−0.482	83

[a] Within our accuracy limitation, this is not significantly different from zero.

$2J$ in Table 2 show that, as the Gd−O distances become more unequal, antiferromagnetic coupling is replaced by ferromagnetic coupling. The sign of the coupling constants in these complexes are correctly reproduced in all four cases, and they are all predicted to have small magnitudes. Further analysis of all the experimental structures reveals magneto-structural correlations in the Gd dinuclear complexes. Both the theoretical results and experimental data show the correlation between the rhombus for the Gd_2O_2 ring and the sign and magnitude of magnetic coupling.

While it is reassuring that we obtain generally good agreement between computed coupling constants experimental data for the complexes thus far considered, the magnitudes of these couplings are quite small. With net couplings of such small magnitude, it is difficult to extract any qualitative chain of reasoning that "explains" the results discussed so far. Furthermore, it seems likely that, as long as we remain focused on hard, saturated oxygen-based donors as bridging ligands, strategies for increasing the magnitude of the Gd−Gd coupling will remain obscured. We therefore turn our attention to dinuclear lanthanide complexes synthesized in Evans' group: those containing diazenido bridges and lower Gd^{III} coordination numbers.

Dinitrogen Complexes

Evans and co-workers have synthesized a class of molecules in which Ln centers are coordinated by two bis(trimethylsilyl)-amide ligands and a single THF molecule: $\{[(Me_3Si)_2N]_2(thf)Ln\}_2(N_2)$; ($Ln^{III}$ = Gd, Tb, Er, Ho, Y, Lu, Tm, Dy, Nd) as shown in **2**.[84−86]

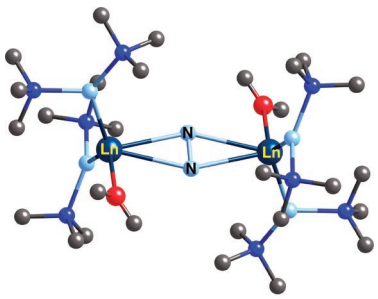

2. Ln = Gd, Tb, Er, Ho, Y, Lu, Tm, Dy, Nd

These molecules have a structure in which dinitrogen bonds in a μ-η^2:η^2-N_2 fashion where the N−N distances are 1.258−1.305 Å, indicating that the bridging dinitrogen is most appropriately described as a diazenido ligand, N_2^{2-}. Despite the fact that the synthesis of some of these compounds involved divalent lanthanide reagents (in the case of thulium, dysprosium, and neodymium), *all* the lanthanide centers in this set of molecules should be regarded as trivalent with $4f^n$ ($n_{La} = 0$, $n_{Ce} = 1$, etc.) core configurations and bearing a 3+ core charge. The same valence description applies to a second class of diazenido-bridged complexes wherein two *tert*-butoxide ligands and two THF molecules are bound to each lanthanide center: $[(2,6\text{-}{}^tBu_2C_6H_3O)_2(thf)_2Ln]_2((\mu\text{-}\eta^2\text{:}\eta^2\text{-}N_2)$ with Ln^{III} = Tm, Dy, Nd.

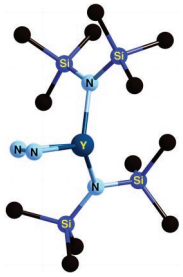

Figure 4. $\{[(Me_3Si)_2N]_2(thf)Ln\}_2(N_2)$; the thf ligand is omitted.

Most lanthanide compounds are 8- or 9-coordinate; the Ln centers in both classes of complex are 5- and 6-coordinate. These relatively low Ln coordination numbers are important in stabilizing the diazenido ligand in these complexes (Figure 4, only half of the dinuclear complex is shown).

Importantly, this relative coordinative unsaturation is compensated by the π-donation of amide and by back-donation from the diazenido ligand. Thus, the ligand bulk, low coordination numbers, and bridging diazenido ligands are interrelated. As we shall see, these circumstances conspire to enhance the magnetic coupling of Gd centers through the bridge.

Yttrium Geometry Optimization. A geometry optimization on the yttrium complexes revealed only minor differences between optimized and experimental structures. All relevant bond distances and angles are shown in Table 3. The computed dinitrogen distance (1.256 Å) is about 1% shorter than observed experimentally (1.268(3) Å), and the computed Y−N distances (2.340 and 2.369 Å) are about 2% longer than those observed experimentally (2.296(2) Å and 2.317(2) Å). All other metal−ligand distances are slightly longer (0.03 Å) than experiment, and the largest discrepancy in bond angles is ∼2°. There are no precedents in the literature to which we can draw comparisons for yttrium complex geometry optimizations using BLYP functional, but bond distances for tris(bis-dimethylsilyl)amido samarium using the hybrid B3LYP functional are also slightly longer than experiment for lanthanide systems.[88−93] All angles

(82) Hou, H.; Li, G.; Li, L.; Zhu, Y.; Meng, X.; Fan, Y. *Inorg. Chem.* **2003**, *42*, 428.
(83) Plass, W.; Fries, G. *Z. Anorg. Allg. Chem.* **1997**, *623*, 1205.
(84) Evans, W. J.; Zucchi, G.; Ziller, J. W. *J. Am. Chem. Soc.* **2003**, *125*, 10.
(85) Evans, W. J.; Lee, D. S.; Ziller, J. W. *J. Am. Chem. Soc.* **2004**, *126*, 454.
(86) Evans, W. J.; Lee, D. S.; Rego, D. B.; Perotti, J. M.; Kozimor, S. A.; Moore, E. K.; Ziller, J. W. *J. Am. Chem. Soc.* **2004**, *126*, 14574.
(87) A more complete table is included in the Supporting Information.
(88) Maron, L.; Eisenstein, O. *J. Phys. Chem. A* **2000**, *104*, 7140.
(89) Maron, L.; Eisenstein, O. *New J. Chem.* **2001**, *25*, 255.
(90) Clark, D. L.; Gordon, J. C.; Hay, P. J.; Martin, R. L.; Poli, R. *Organometallics* **2002**, *21*, 5000.

Table 3. Selected Experimental and DFT Optimized Bond Distances (Å) and Angles (deg) for $\{[(H_3Si)_2N]_2(solv)Y\}_2(N_2)^{0,+1}$ [87]

	experimental geometry	geometry optimization	1-e⁻ oxidation
	Bond Distances (Å)		
Y−N3 (diazenido)	2.2958(7)	2.340	2.502
Y−N4	2.3170(16)	2.369	2.537
N4−N3	1.268(3)	1.256	1.182
Y−O			
thf	2.3898(14)	2.487	2.368
OMe_2[a]	2.465	2.487	2.411
H_2O[a]	2.504	2.470	2.430
	Bond Angles (deg)		
N3−Y−N4 (diazenido)	31.90(8)	30.94	27.12

[a] Experimental Ln−OMe_2 and Ln−H_2O distances were determined from partial geometry optimizations varying only the Ln−Solv distance.

Table 4. Comparison of Overall Mulliken Charges and Populations, and Percent SFO Populations of Various Atomic Orbitals for Experimental and DFT Geometry-Optimized Structures for $\{[(H_3Si)_2N]_2(thf)Y\}_2(N_2)$

	geometries	
	experimental	optimized
	Y−N (Diazenido) Distance (Å)	
Y−N3	2.2958(17)	2.340
Y−N4	2.3170(16)	2.369
	Mulliken Charges	
Y	1.7763	1.8014
N	−0.4710	−0.5038
	Orbital Populations	
Y 4*d*	1.0661	1.0021
N 2*s*	1.7583	1.7547
N 2*p*	3.6418	3.6776
	SFO Gross Population (%)[a]	
HOMO (eV)	−4.121	−3.931
N−*p*	67.33	68.28
Y−*d*	21.88	23.38
LUMO (eV)	−2.698	−2.525
N−*p*	86.61	86.38
Y−*d*	8.13	8.10

[a] SFO = Symmetry adapted combination of fragment orbitals.

and bond lengths in the disilylamide ligands are normal; there are no indications that would suggest that C−H bonds are donating significantly to the Y centers. We therefore replaced the $Si(Me)_3$ groups with simpler SiH_3 groups in our calculations.

To better assess the effect that the experimental and calculated metal−diazenido distances have on bonding in the Ln_2N_2 core, relevant Mulliken charges and populations are shown in Table 4. First, it appears that there is a modestly greater charge separation for the optimized geometry than for the experimental geometry. Population analysis shows greater overall Y *d*-electron density at the experimental structure, indicating a potential underestimation of back-bonding from the diazenido bridge to the yttrium in the optimized structure.[94]

Calculated Gd Exchange Coupling. The calculated values of *J* for $\{[(Me_3Si)_2N]_2(thf)Gd\}_2(N_2)$ and models $\{[(H_3Si)_2N]_2$-$(Solv)Gd\}_2(N_2)$ with different solvent ligands are presented in Table 5. For both geometries, calculations predict antiferromagnetic couplings that, while weak, are significantly stronger than those for the oxygen-bridged complexes. Caution is advisable in drawing quantitative conclusions since we see significant variations in computed *J* values when the geometric details of the structures are also varied. In addition, changes in the oxygen donors (H_2O, $O(Me)_2$, and THF) exert little effect on the computed *J* coupling constant. We are particularly interested in whether ligands with unpaired delocalized electrons might effectively couple lanthanide magnetic moments. With this in mind, we performed calculations for a 1-electron-oxidized complex, $\{[(Me_3Si)_2N]_2(thf)Y\}_2(N_2)^{+1}$. There is, as yet, no experimental evidence for the existence of such species; as a result, we performed a geometry optimization on the $N(SiH_3)_2$ derivative complex, then varied the solvent ligand, keeping the core structure fixed. Not surprisingly, upon oxidation the N−N distance shortened to 1.182 Å ,and the Y−N distances was lengthened to 2.602 and 2.560 Å. The computed distances in the latter are probably too long since they were too long in the neutral parent molecule. Replacing Y with Gd, the calculated *J* values for the different model structures are shown in Table 5. The results show that the compounds favor ferromagnetic exchange with much stronger coupling than for the neutral molecule. Again, changing solvent ligands yielded only slight changes in the magnitude of computed coupling constant. Previous researchers have correlated changes in exchange coupling constants with the basicity of nitrogen-containing terminal ligands in hydroxo-bridged copper (II) binuclear complexes, but from among the computational variations we have investigated, we find no obvious correlations between the pK_a of the solvent molecules and magnetic couplings.[57,95−98]

Table 5. Calculated Exchange Coupling Constant (J/cm^{-1}) and Gd Mulliken Populations of the Complexes $\{[(R_3Si)_2N]_2(Solv)Gd\}_2(N_2)^n$ (R = Me, H) (n = 0, +1), with Various Solvent Ligands

		s–*d* Mulliken populations		
		P_{BS}[b]		P_{HS}[c]
compound	J(cm^{-1})	$4f^{\uparrow}$	$4f^{\downarrow}$	$4f^{\uparrow}$
	Experimental			
$[\{[(Me_3Si)_2N]_2(thf)Gd\}_2(N_2)]$	−0.112	0.142	0.142	0.132
$[\{[(H_3Si)_2N]_2(Solv)Gd\}_2(N_2)]$[a]				
OMe_2	−0.042	0.151	0.151	0.141
thf	−0.048	0.151	0.151	0.144
H_2O	−0.055	0.152	0.152	0.143
	Geometry Optimization			
$[\{[(Me_3Si)_2N]_2(thf)Gd\}_2(N_2)]$	−0.129	0.143	0.143	0.133
$[\{[(H_3Si)_2N]_2(Solv)Gd\}_2(N_2)]$				
OMe_2	−0.188	0.153	0.153	0.142
thf	−0.203	0.154	0.154	0.142
H_2O	−0.207	0.155	0.155	0.143
	1-Electron-Oxidized Species			
$[\{[(H_3Si)_2N]_2(Solv)Gd\}_2(N_2)]^{+1}$				
OMe_2	2.74	0.196	0.054	0.197
thf	2.64	0.201	0.056	0.197
H_2O	2.95	0.200	0.060	0.197

[a] Uses an experimental distance for Si−H = 1.350 Å. Gd−OMe_2 and Gd−H_2O distances were determined from partial geometry optimizations varying only the Gd−Solv distance. [b] P_{BS}: Summed 6*s* and 5*d* spin populations for the broken symmetry calculation, $|\uparrow_7,\downarrow_7\rangle$. [c] P_{HS}: Summed 6*s* and 5*d* spin populations for the high spin calculation, $|\uparrow_7,\uparrow_7\rangle$.

(91) Eisenstein, O.; Hitchcock, P. B.; Khvostov, A. V.; Lappert, M. F.; Maron, L.; Perrin, L.; Protchenko, A. V. *J. Am. Chem. Soc.* **2003**, *125*, 10790.
(92) Perrin, L.; Maron, L.; Eisenstein, O.; Lappert, M. F. *New J. Chem.* **2003**, *27*, 121.
(93) Brady, E. D.; Clark, D. L.; Gordon, J. C.; Hay, P. J.; Keogh, D. W.; Poli, R.; Scott, B. L.; Watkin, J. G. *Inorg. Chem.* **2003**, *42*, 6682.
(94) A geometry optimization on a model for $[(2,6\text{-}^tBu_2C_6H_3O)_2(thf)_2Y]_2(N_2)$ produces similar results: N−N and Y−N computed distances were 1.255 Å and 2.346 Å/2.361 Å, respectively. The yttrium analogue of the aryloxide complex has not been synthesized; therefore, no comparison can be made, and our discussion will focus on the disilylamide complex.
(95) Arnett, E. M.; Wu, C. Y. *J. Am. Chem. Soc.* **1960**, *82*, 4999.
(96) Arnett, E. M.; Wu, C. Y. *J. Am. Chem. Soc.* **1962**, *84*, 1684.

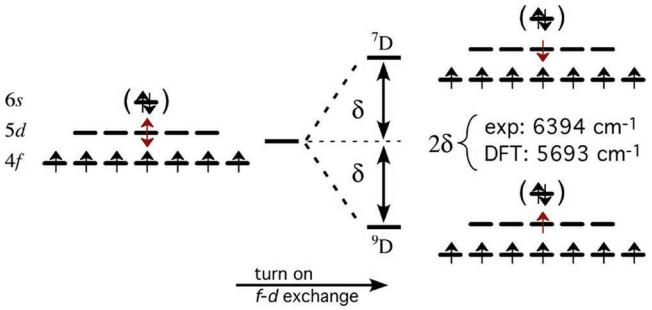

Figure 5. Electronic splitting of Gd atom as a function of 4*f*−5*d* exchange perturbation.

Interpretation of the Results

The $4f^7$-exchange field can be viewed, to a good approximation, as a kind of *contact* interaction—exerting its *direct* influence only on orbitals centered on the Gd atom. The valence 5*d* and 6*s* electrons penetrate to some extent into the atomic core, where they experience the effect of this exchange field. The more contracted 5*d* electrons penetrate to a greater extent than the 6*s* electrons and, consequently, experience greater exchange interaction with the $4f^7$ core. This local character of the $4f^7$-exchange field suggests that a simple perturbative molecular orbital (PMO) model can be used to model the perturbation that the $4f^7$ cores exert on electrons that reside in molecular orbitals with 5*d*- and 6*s*-character—and thereby controls magnetic exchange couplings in polynuclear Gd compounds. In previous papers, we've described our perturbative model, which is outlined as follows.[64,99]

First, consider an "unperturbed" system: a Gd atom with a $4f^75d^16s^2$ configuration and *in the presence of an "averaged" 4f−5d exchange interaction* (Figure 5). In this hypothetical situation, the 5*d* electron experiences an average exchange field effect from the $4f^7$ half-shell and has no preferred spin orientation. Upon applying the exchange field, a *d*-electron spin aligned with (against) the $4f^7$ spins is stabilized (destabilized) by an energy δ. For a Gd atom, 2δ is just the difference between the ^{9}D and the first excited state, ^{7}D, computed to be 0.706 eV in our calculations (see above). In essence, the PMO model assumes that this exchange perturbation is exerted on any valence MO via the 5*d* electron contribution to that MO for a given molecule (or solid). Thus, the "unperturbed" MOs are identical for spin-up and spin-down electrons, and the arrangement (spin pattern) of Gd moments perturbs these MOs, (de)stabilizing them when their 5*d*-spin density spreads over Gd centers with like (different) 4*f* spin density. The net (de)stabilization conferred on the delocalized electrons by competing 4*f* spin patterns determines the energetic ordering of the spin patterns.

***d*-Electron-Mediated Exchange.** We can treat the Gd diazenido dimer model in the same spirit just described and adopt a simple *d*-metal−*p*-ligand bonding scheme to account for the frontier molecular orbitals of this bonding system. Shown in Figure 6 is a molecular orbital diagram for the Gd_2N_2 moiety. Only the Gd−N bonds are drawn; the MOs are given D_{2h} representation labels, although that symmetry is only approximate. Figure 7 shows a perturbative analysis using these

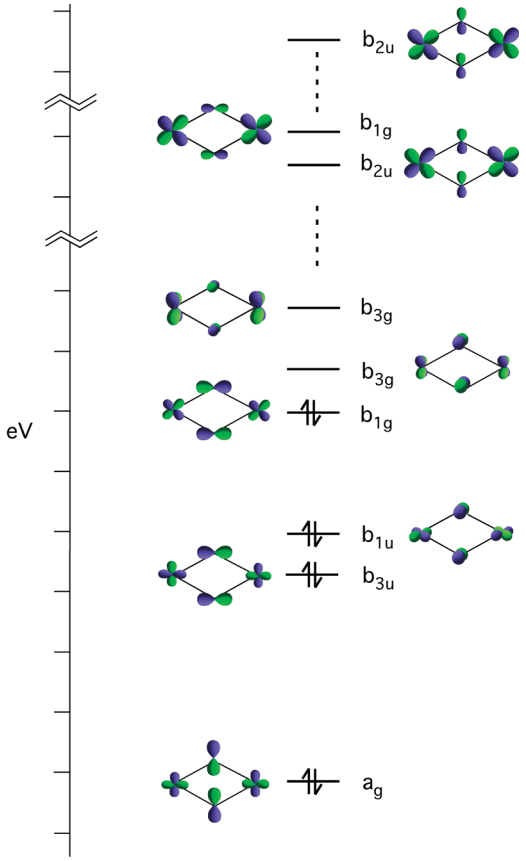

Figure 6. Molecular orbital diagram for the Gd_2N_2 moiety. Also shown are the pertinent unoccupied orbitals.

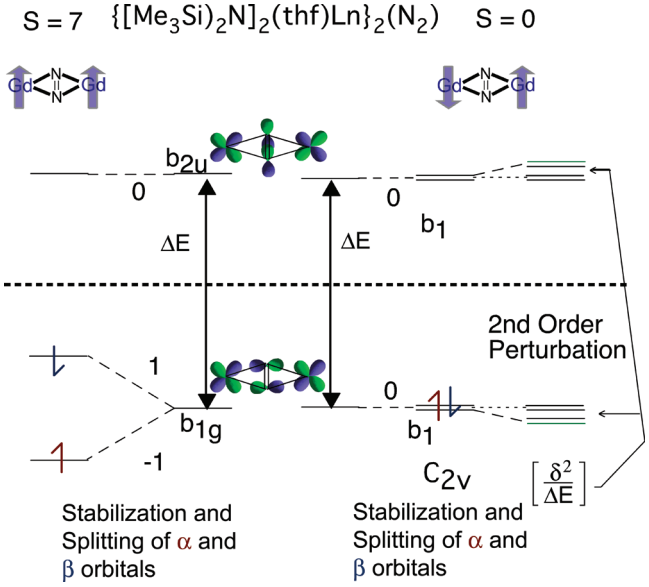

Figure 7. Treatment of the exchange interaction in $\{[(H_3Si)_2N]_2(thf)Gd\}_2(N_2)$ as a second-order perturbation to the system.

Gd_2N_2 orbitals. ΔE represents the gap between the HOMO and the higher-lying antibonding orbitals. Orbital plots shown in Figure 8 clearly demonstrate that appreciable *d*-electronic character in the HOMO—underlining the plausibility of this treatment.

In the all-spin-aligned $S = 7$ case, the 4*f* moments induce a first-order splitting in the α- and *β*-spin molecular orbitals. Because the symmetry of the exchange potential felt by the Gd

(97) Arnett, E. M.; Wu, C. Y. *J. Am. Chem. Soc.* **1962**, *84*, 1680.
(98) Okada, M.; Suyama, K.; Yamashita, Y. *Tetrahedron Lett.* **1965**, 2329.
(99) Roy, L. E.; Hughbanks, T. *Mater. Res. Soc. Symp. Proc.* **2002**, *755*, 25.

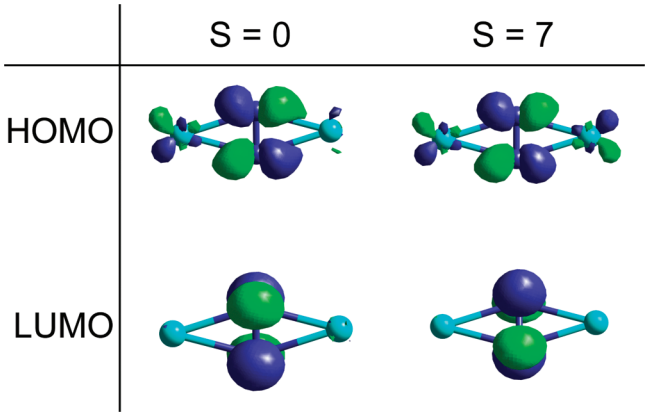

Figure 8. HOMO and LUMO orbital plots for $\{[(Me_3Si)_2N]_2(thf)Gd\}_2(N_2)$ $S = 0$ and $S = 7$ (disilylamide and THF ligands omitted for clarity).

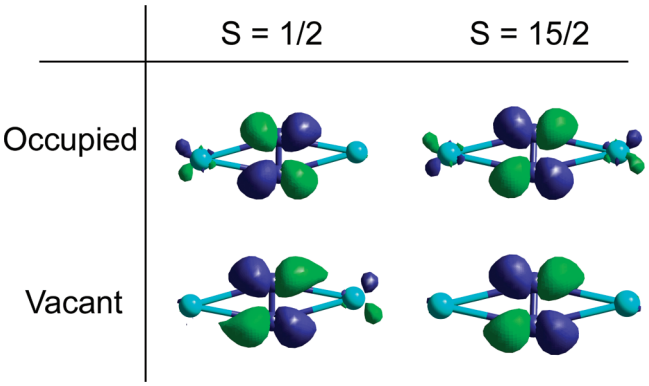

Figure 9. HOMO and LUMO orbital plots for $[\{[(Me_3Si)_2N]_2(thf)Gd\}_2(N_2)]^{1+}$ $S = {}^1/_2$ and $S = {}^{15}/_2$ (Gd and N atoms only shown for clarity).

5*d* and 6*s* electrons is unchanged, no second-order mixing occurs among orbitals of different symmetry. When the 4*f* moments are oppositely oriented, the exchange potential felt by the 5*d* and 6*s* electrons has a reduced (near-C_{2v}) symmetry. Mixing between the HOMO and frontier MOs is thereby induced, yielding a second-order stabilization of both α and β spins (manifest in polarization of each electron toward its like-spin $4f^7$ center).

The default expectation for a closed *d*-shell system is antiferromagnetic coupling because antiferromagnetic $4f^7$-spin patterns inherently *break orbital symmetry for each spin* and will mix unoccupied orbitals into the occupied orbitals of like spin, allowing for stabilization via spin polarization. Indeed, in any otherwise-closed-shell system, f^7 spin ordering that is effective at inducing 5*d*/6*s* spin polarization will tend to have lower energy because such spin polarization always reflects the fact that the delocalized electrons spend more time in the vicinity of like-spin *f*-electrons.

The one-electron oxidized case is clear-cut: the unpaired delocalized electron is stabilized in first order with its spin aligned with both 4*f* moments, and the magnitude of the stabilization is much greater than that seen for the second-order effects. The effects of polarization can be seen in the orbital plots in Figure 9 for the $S = {}^{15}/_2$ spin state vs the $S = {}^1/_2$ spin pattern.

Spin Density Distribution. The preceding analysis reveals a direct correlation between the sign and magnitude of the exchange coupling constant when examining the Mulliken spin densities on both the bridging atoms and the metal. It is instructive to examine the spin density distribution for the disilylamide Gd dimer complex (i.e. the local differences in α- and β-spin populations). The most relevant atomic spin densities obtained from our calculations are presented in Table 5. For both spin patterns, the 5*d* and 6*s* Gd spin polarizations mirror the spin orientations of $4f^7$ core. We have given the magnitudes in Table 5. We have combined 5*d* populations with 6*s* populations because they track with each other; the 6*s* polarization is consistently about 2.3 times smaller than that for the total 5*d* populations. The data in Table 5 confirm our perturbation-theoretic interpretation. For the closed-shell system, the symmetry-breaking antiferromagnetic pattern induces a much greater spin polarization than is seen in the ferromagnetic case. In the one-electron case, the spin density shows that the unpaired spin is polarized to its like-spin gadolinium neighbor.

Conclusion

We have pioneered the use of the broken symmetry approach for the analysis of the magnetic coupling in rare-earth compounds.[64,99] The method complements experimental studies in elucidating the compositional and structural origins of magnetic ordering in rare-earth magnetic materials. Computed magnetic coupling constants are in good agreement with the reported values for the oxygen-bridged Gd^{III} compounds, supporting the reliability of this treatment. Moreover, we have applied a perturbative-theoretic technique using the diazenido-bridged Gd^{III} complexes, which underline the plausibility of this treatment.

In the diazenido system, the ferromagnetic exchange field is totally symmetric in D_{2h} symmetry; in the antiferromagnetically coupled molecule, the exchange field lowers the spin-dependent symmetry experienced by the delocalized electrons to C_{2v}. However, because this perturbation does not couple the HOMO and LUMO, dramatically larger Gd−Gd exchange coupling is precluded. The perturbative analysis suggests that the best strategy for obtaining strongly coupled lanthanide magnetic molecules (solids) consists of finding ligands that effectively minimize the energy gap between the frontier and adjacent orbitals and that mix in some significant Ln 5*d* character to the same to yield strongly (ferro- or antiferromagnetically) coupled systems. Complexes with open valence shells—with appreciable unpaired spin density delocalized into Ln 5d acceptor orbitals—should exhibit even stronger coupling. We are currently examining model systems where such coupling can occur.

Acknowledgment. We thank Dr. Lisa Perez and Prof. Michael Hall for valuable help and discussions. We thank the Robert A. Welch Foundation for its support through Grant A-1132 and the Texas Advanced Research Program through Grant 010366-0188-2001. We also thank the Supercomputing Facility at Texas A&M and the Laboratory for Molecular Simulation for computing time and other support.

Supporting Information Available: Complete ref 71, calculated charges and net spin densities for models of $[Gd(AmPh)]_2$ and $[\{Gd(O_2CR)_3(H_2O)_2\}_2]$, and selected experimental, DFT-optimized, and 1-e-oxidized bond distances (Å) and angles (deg) for $\{[(Me_3Si)_2N]_2(thf)Y\}_2(N_2)$. This material is available free of charge via the Internet at http://pubs.acs.org.

JA055035J